VOL. 14, NO. 14, JULY 2019 ISSN 1819-6608
ARPN Journal of Engineering and Applied Sciences

www.arpnjournals.com

EXAMINATION OF THE RELEVANT OF THE FREQUENCY RESPONSES AND THE PERFORMANCE FOR THE DEVISED PIEZOELECTRIC POWER GENERATOR WITH THE STIFFNESS OF THE VIBRATING BEAM

N. X. Yan[1], A. A. Basari, K. S. Leong, N. A. A. Nawir and S. Hashimoto[2]
[1]Centre for Telecommunication Research and Innovation (CeTRI), Faculty of Electronics and Computer Engineering (FKEKK), Universiti Teknikal Malaysia Melaka (UTeM), Durian Tunggal, Melaka, Malaysia
[2]Division of Electronics and Informatics, School of Science and Technology, Gunma University, Kiryu-shi, Gunma, Japan
E-Mail: xueyan093@gmail.com

ABSTRACT

The frequency responses and the output efficiency of the piezoelectric disc by the designed piezoelectric power generator are examined and vindicated in this paper. The relationship between the stiffness of a beam with the output efficiency and the frequency responses of the piezoelectric disc are investigated. As the vibrating beam's bending stress is varied, the impact force is affected and changed. Two variables such as width and thickness of the vibrating beam are disclosed. The narrower the width of the vibrating beam, the higher the frequency responses (shifted to right region) of the piezoelectric disc. Approximately 87% of the output efficiency of the piezoelectric disc is raised when 1mm of the vibrating beam's thickness is employed on the power generator contrast with the 2mm of the vibrating beam's thickness. In this paper, the declarations are expounded and evaluated from the plotted graphs.

Keywords: stiffness of the beam, vibration-based impact mode, energy harvester, piezoelectric power generator, piezoelectric disc.

1. INTRODUCTION

One of the contemporary trends is the Industry 4.0 of the wireless sensor network (WSN). Yet, due to the inconvenience of the battery to the WSN nodes which is caused by the short-lifetime and the substitution or reloading the battery [1]–[3]. Therefore, energy harvesting can be considered in order to transform the ambient waste energy into electrical energy and reduce the usage of battery, has been interested by the researchers [1]. Solar energy, mechanical energy, thermal sources, vibrational energy and human motion are some of the ambient sources [3], [4]. The energy that is yielded from the ambient sources can function the small-scale system such as WSN [4], [5].

There are some variations of the vibration energy harvester which are used for the energy conversion principle: piezoelectric, magnetostriction, electrostatic and electromagnetic [4]-[7]. The capability of a transducer that can transform kinetic or vibration energy into electricity is defined as the energy conversion principle. As the piezoelectric transducer has the behavior of coupled electromechanical and high density of energy. Thus, the piezoelectric transducer becomes first considered contrast with others [6].

Yet, the bandwidth of the operating frequency of the piezoelectric transducer is comparatively narrow because of the quality factor which is also acknowledged as Q-factor of the piezoelectric transducer is high [8]. Thus, the output efficiency only can be obtained within the small range of the operating frequency. The yielded output efficiency is decreased dramatically when the resonant frequency of the piezoelectric transducer is far away from the natural frequency. Hence, the resonant frequency of the piezoelectric transducer is required to be evaluated and regulated so it is corresponding with the environment frequency in order to yield high output efficiency.

Three main factors have been centralized in the literatures to study and examine the frequency response of the piezoelectric: length of the piezoelectric cantilever [8]-[10], thickness of the piezoelectric cantilever [11] and the width of the piezoelectric cantilever [12]. Bong Yu Jing *et al*. justified that the resonant frequency of the piezoelectric cantilever is increased (shifted to right region) when the stiffness of the piezoelectric cantilever is increased while the length of the piezoelectric cantilever is decreased which is reported in [10]. The investigation of the frequency responses and the performance of the piezoelectric cantilever by varying the thickness of the piezoelectric cantilever is discussed in [11]. Moreover, the shape of the piezoelectric cantilever also been studied to investigate the frequency response and harvest a higher performance [13]–[16]. However, these methods are employed on the piezoelectric cantilever only to study the performance and frequency responses of the piezoelectric. They are not incorporated with the structural of the piezoelectric power generator.

Thereupon, the influence of the stiffness of a vibrating beam to the performance and the frequency responses of the piezoelectric disc is examined through applying the beam on a designed piezoelectric power generator. The behavior of the piezoelectric disc with the interfaced plate through a free fall experiment and continuous vibration experiment are described in [17] and [18], [19], respectively. Hence, the properties of the vibrating beam stiffness with the devised piezoelectric power generator are evaluated and examined. Two variables of the vibrating beam are analyzed which are the width and thickness of the vibrating beam. The justification and clarification of the parameters can be

used to the research of the vibration-based impact mode piezoelectric energy harvester.

2. STIFFNESS AND STRENGTH

The strength of materials or mechanics of materials is determined as the aspects of an object that is disclosed to stress and strain. Stress is occurred when an object material is charging by an applied force. Whereas, the response of an object material, for example the object's shape is altered is known as strain. Therefore, the stress and strain are associated with the object material's response. While stiffness is defined as an object shape is varied by a resistance. When the stress is disappeared, the object material will be rehabilitated to its original shape with the present of the object stiffness. The resistivity of the object material to endure the deformation or overshoot is determined as strength. Hence, the stiffness and strength are appertained to the behavior of the object material [20]. The correlation of the stiffness and yield strength is illustrated in Figure-1 which is a stress-strain curve. The gradient of the stress to strain is the stiffness which also called as the elastic coefficient of the object material. The strength of the object material is demonstrated from the stress applied.

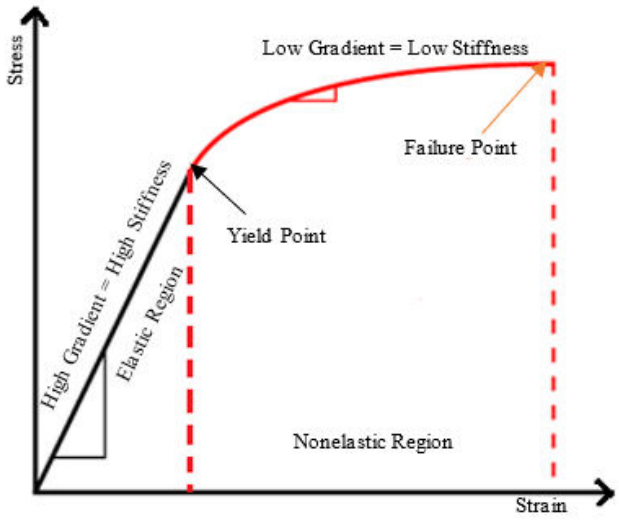

Figure-1. A stress-strain curve.

Figure-2 demonstrates the stiffness of the different materials with a force-extension curves. The higher the gradient, k, the higher the stiffness of the material.

The stiffness can be derived as Equation (2.1).

$$K = \frac{F}{\delta} \tag{2.1}$$

Where,

K = The stiffness,
F = The applied force, and
δ = The deformation.

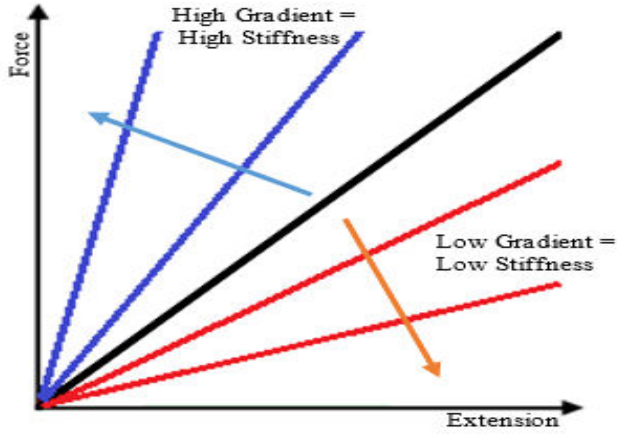

Figure-2. The force-extension curve that is illustrating the stiffness of a material.

One side of a metal surface is lengthened familiarly during the metal piece is meandering. Meantime, the other side of the metal surface is squeezed. Between the two surfaces of the object material have a line of zero stress and it is known as the neutral axis. The pressure and density for the balanced, unstressed and the Young's modulus of the object material are alike when the commencing condition of the beam is unbent. The bending stress and the flexural modulus can be modelled as Equations (2.2) and (2.3).

$$\sigma_b = \frac{3PL}{2wt^2} \tag{2.2}$$

$$E_b = \frac{PL^3}{4wt^3y} \tag{2.3}$$

Where,

σ_b = Bending stress,
E_b = Flexural modulus,
P = Normal force,
l = Length of the beam,
w = Width of the beam,
t = Thickness of the beam, and
y = The deflection at load point.

The flexural modulus E_b is interpreted as the initial modulus from the stress-strain curve in pressure. So, the maximal beam surface stress farthermost from the neutral axis can be equaled as Equation (2.4).

$$\sigma_{max} = \frac{Mc}{I} = \frac{M}{Z} \tag{2.4}$$

Where,

σ_{max} = The maximal beam surface stress,
M = The moment of bending,
c = The distance between neutral axis and outer surface,
I = The inertia moment, and
Z = I/c = The section modulus.

The relevancy of the maximal cantilever beam surface stress with an intermediary load at one end can be interpreted as Equation (2.5).

$$\sigma_{max} = \frac{3dEt}{2l^2} \quad (2.5)$$

Where,
σ_{max} = The maximal cantilever beam surface stress,
d = The beam deflection,
E = The elasticity modulus,
t = The thickness of the beam, and
l = The length of the beam.

When varying the beam outline, the strain energy is required to be ensured in the beam constant for the purpose of decreasing the maximal stress.

3. DEFLECTION OF THE BEAM

When a structural composition is applied by a load, the difference of the distance or angle in degree is known as deflection. The deflected shape's slope of a loaded object can be affected by the deflection distance of the loaded object. Beams can be changed in their element and geometry. When a force is applied, a beam will be curved, prolong, or straighten which will be affected in x-axis or y-axis. The deformation of the beam is linear elastic deformation, and the deflection of the beam is small when a force is applied. A cantilever beam is long, slight and straight.

An end-loaded cantilever beam is occurred when one end of the cantilever beam is fixed. The deflection and incline of the fixed end cantilever beam is zero. A cantilever beam with one end fixed is illustrated in Figure-3. The elastic deflection of the cantilever beam and the deflection angle can be expressed as Equations (3.1) and (3.2).

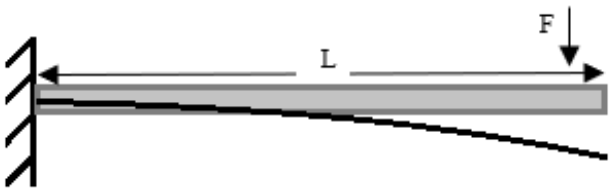

Figure-3. Cantilever beam's deflection when a force is applied on the end of the cantilever beam.

$$\delta_B = \frac{FL^3}{3EI} \quad (3.1)$$

$$\emptyset_B = \frac{FL^2}{2EI} \quad (3.2)$$

Where,
δ_B = The elastic deflection of the cantilever beam,
$\emptyset_B$ = The deflection angle of the cantilever beam,
F = Applied force,
L = Beam length,
E = Elasticity modulus,
I = Area moment of inertia.

However, the deflection of the beam is increased eight times larger when the beam length is doubled. The deflection of point x on the end loaded cantilever beam can be expressed as Equations (3.3) and (3.4).

$$\delta_x = \frac{Fx^2}{6EI}(3L - x) \quad (3.3)$$

$$\emptyset_x = \frac{Fx}{2EI}(2L - x) \quad (3.4)$$

Where,
$\delta_x = \delta_B$ = The elastic deflection of the cantilever beam,
$\emptyset_x = \emptyset_B$ = The deflection angle of the cantilever beam,
x = The end of the beam length.

4. ANGULAR ACCELERATION, ANGULAR VELOCITY AND ANGULAR DISPLACEMENT

The difference angle that is revolved about a particular axis which is in unit radians from a point is appraised as angular displacement. It is used to refer the distance of an object shifts in a camber path and the arc length of the camber path. The angular displacement can be presented as Equation (4.1).

$$\theta = \frac{S}{r} \quad (4.1)$$

Where,
θ = The angular displacement,
S = The linear displacement, and
r = The curvature's radius.

While the computation of the object's speed is varying its angle is determined as angular velocity. The angular acceleration is the computation of the object's speed is varying its angular velocity. The angular velocity and the angular acceleration can be modelled as Equations (4.2) and (4.3).

$$\omega = \frac{v}{r} \quad (4.2)$$

$$\alpha = \frac{a_t}{r} \quad (4.3)$$

Where,
ω = The angular velocity,
α = The angular acceleration,
v = The linear speed,
r = The curved path's radius, and
a_t = The tangential acceleration.

Equations (4.1), (4.2) and (4.3) describe that the angular displacement, angular velocity and angular acceleration are proportional to the linear displacement, linear velocity and tangential acceleration, respectively. Therefore, the angular displacement, angular velocity and angular acceleration can be associated together. By substituting the θ, ω and α for S, v and a_t, respectively into a linear motion equation which is $v_f^2 - v_0^2 = 2aS$. Therefore, the angular motion equation can be equaled as

Equation (4.4).

$$\omega_f^2 - \omega_0^2 = 2\alpha\theta \quad (4.4)$$

Where,

ω_f = The final angular velocity, and

ω_0 = The initial angular velocity.

5. METHODS AND MATERIALS

5.1 Characterize the Stiffness of Vibrating Beam

Firstly, the stiffness of the vibrating beam is analyzed, and the tentative setup is illustrated in Figure-4. There are four values of width of the vibrating beam which are 8mm, 10mm, 12mm and 14mm. Each of them has two different values of thickness which are 1mm and 2mm which is shown in Figure-5. The apparatus and equipment that are used such as electrodynamic shaker function generator, gain amplifier, G-link sensor node and receiver and Portable Digital Vibrometer (PDV) 100. The one end of the vibrating beam is fixed on the electrodynamic shaker. Different G-level of acceleration vibrations are implanted on the electrodynamic shaker as well as the vibrating beam. Hence, the vibrating beam is vibrated according to the set-up acceleration level. The G-link sensor node and receiver are utilized to inspect the acceleration level of the electrodynamic shaker. By using the function generator, AC input power is supplied to the electrodynamic shaker. Yet, a high power is required to supply the electrodynamic shaker for the G-level of acceleration. Thus, the gain amplifier is employed to amplify the power provided from the function generator, since the power supply from the function generator is not ample for the electrodynamic shaker. Then, a stainless-steel ball is dropped 100mm height from another side end of the vibrating beam. At the same time, the deflection of the vibrating beam is measured by using the Portable Digital Vibrometer (PDV) 100.

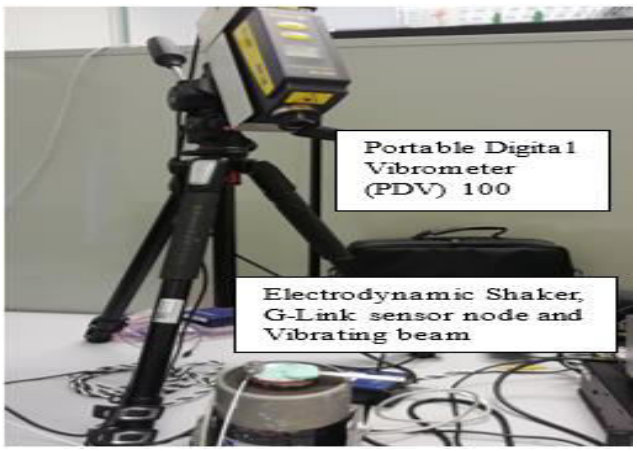

Figure-4. The experiment setup for indicating the vibrating beam's stiffness.

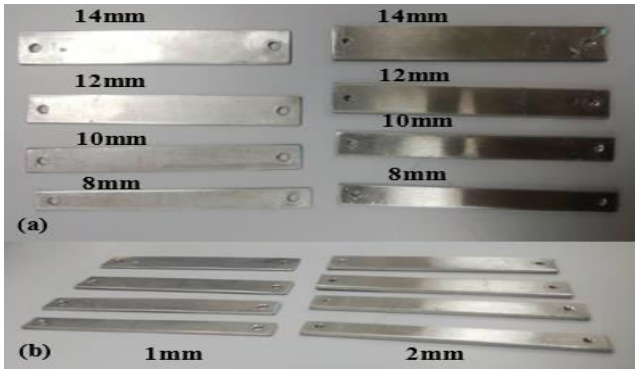

Figure-5. The vibrating beams structures (a) Different widths of vibrating beam (b) Different thickness of vibrating beam.

5.2 The Vibrating Beam is applied on the Power Generator

Afterward, the vibrating beam is applied on a designed piezoelectric power generator as demonstrated in Figures 6 and 7. A setting-based beam, vibrating beam and spacer are included in the power generator. Because of the aluminium is lighter than others material, the setting-based beam and spacer are made up from aluminium. As the elasticity of the aluminium is smaller than the stainless steel, the vibrating beam is made up from stainless steel. For the setting-based beam, there is a 30mm diameter of hole for placing a piezoelectric disc on top of that hole. This is due to the hole can buttress and elongate the piezoelectric disc in a maximal position during the screw tip on the vibrating beam is hitting on the piezoelectric disc. Consequently, it can enlarge the produced output power. Meanwhile, a screw tip and a proof mass are deposed on the end of the vibrating beam. With the assistance of the electrodynamics shaker and proof mass, a 3mm diameter of the screw tip is employed to strike on the piezoelectric disc. Because of the stainless steel is heavier than other elemental in a same dimension, so the stainless steel is applied for the proof mass. While another end of the vibrating beam is fixed with the spacer and setting-based beam. In order to enhance and maximize the produced output power of the piezoelectric disc, an interfaced plate is enclosed on the piezoelectric disc. Due to there is an interfaced plate is positioned between the vibrating beam and setting-based beam, a separator which is functioned by the spacer is applied between them. The sizes and aspects of the piezoelectric power generator for setting-based beam, vibrating beam and spacer are demonstrated in Table 1. An external drive type of piezoelectric ceramic disc, 7BB-35-3L0 is adopted in this tentative. It is assembled by Murata Manufacturing Co., Ltd. The particulars of the piezoelectric disc are expounded in Table 2. The conformation of piezoelectric ceramic disc is displayed in Figure 8.

The experiment setup for applying the vibrating beam on the piezoelectric power generator is demonstrated in Figures 9 and 10. The electrodynamic shaker, gain amplifier, G-link sensor node and receiver, and function generator still are used for the power generator

experiment. The others apparatus and equipment are utilized which are DEWESoftX2, digital storage oscilloscope and decade resistance box. The one end of the devised piezoelectric power generator is regulated on the electrodynamic shaker. 1 G-level of the acceleration is set up and furnished to the electrodynamic shaker. Meantime, the vibrating beam is vibrated and contacted with the piezoelectric disc then produced output efficiency. With the aids of the DEWE Soft X2 software, the electrodynamic shaker's acceleration level can be observed. The load resistance for the piezoelectric disc is intention by the decade resistance box, Cratech UK. The output efficiency of the piezoelectric disc is yielded by varying the different values of width and thickness of the vibrating beam. The digital storage oscilloscope is utilized to observe the continuous produced output efficiency.

As the different values of gap between the screw tip with the piezoelectric disc can influence the harvested output efficiency, so each variables and factors for this experiment will be implemented three times. The output efficiency reading is the average of the three total output efficiency readings. Therefore, the average output efficiency of the piezoelectric will be more precise by replicating the experiment.

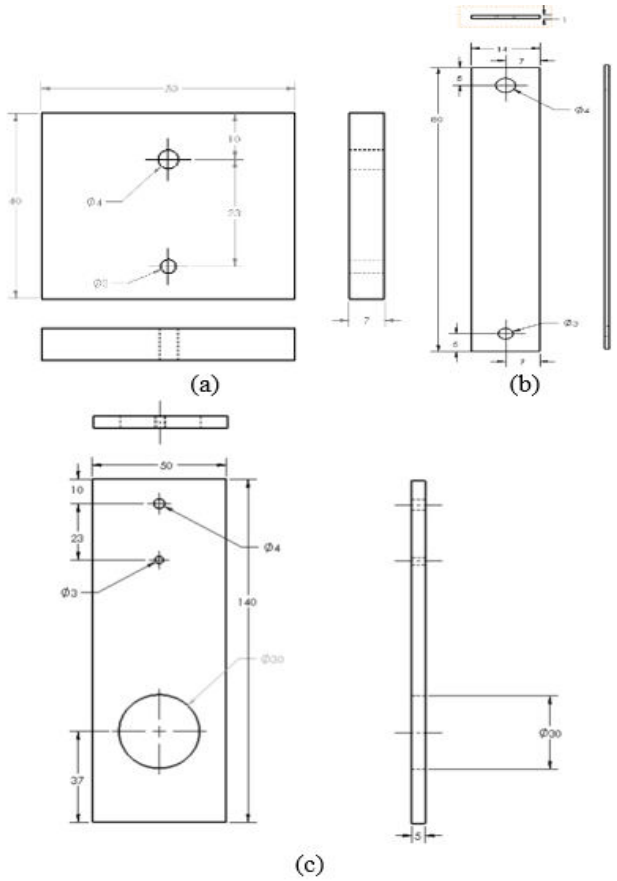

Figure-6. Dimensions of the devised piezoelectric power generator (a) Spacer (b) Vibrating beam and (c) Setting-based beam.

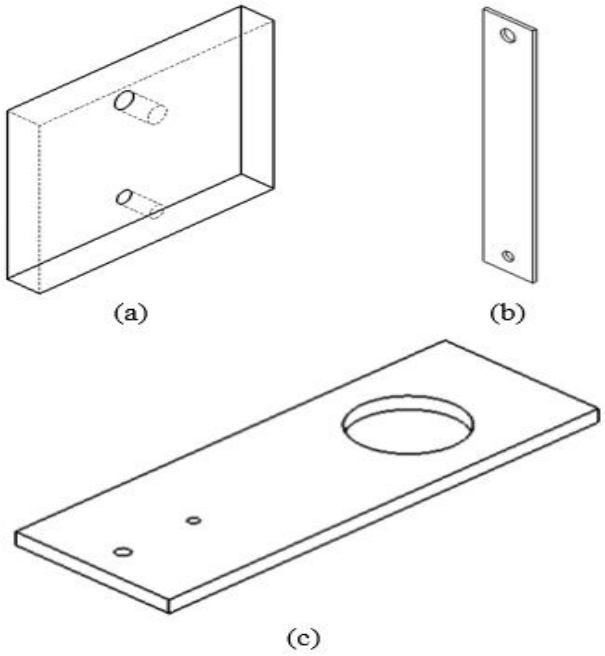

Figure-7. Three-dimensional space of the piezoelectric power generator (a) Spacer (b) Vibrating beam and (c) Setting-based beam.

Table-1. Aspects of the Piezoelectric Power Generator.

Structures	Volume $(W \times L \times H)mm^3$
Setting-based Beam	$50 \times 140 \times 5$
Vibrating Beam	$10 \times 80 \times 1$
Spacer	$50 \times 40 \times 7$

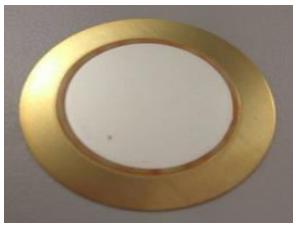

Figure-8. The piezoelectric ceramic disc, 7BB-35-3L0.

Table-2. Details of the piezoelectric ceramic disc, 7BB-35-3L0.

Parameter	Value
Plate diameter (*mm*)	35
Element diameter (*mm*)	25
Electrode diameter (*mm*)	23
Thickness (*mm*)	0.53
Plate thickness (*mm*)	0.30
Resonant Impedance (Ω)	200
Capacitance (*nF*)	$30.0 \pm 30\%$ $(1kHz)$
Plate material	Brass with lead wire

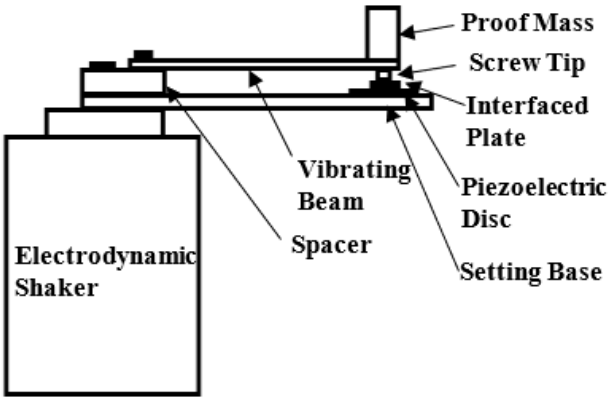

Figure-9. The schematic of the experiment setup for the power generator.

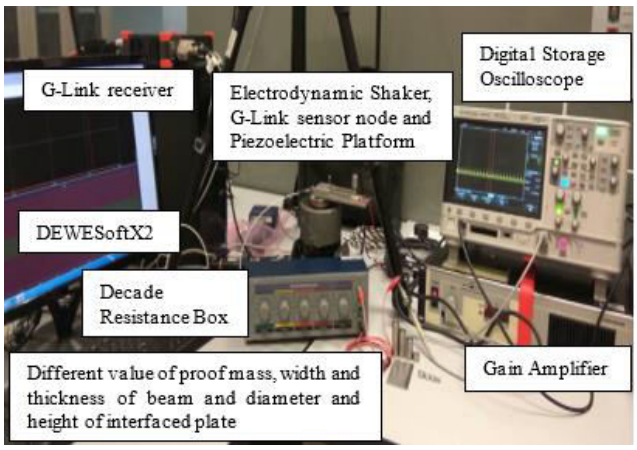

Figure-10. The tentative setup for the power generator experiment.

6. EXPERIMENTAL RESULTS AND DISCUSSIONS

6.1 Characterize the Stiffness of Vibrating Beam

The vibrating beam's stiffness is characterized by changing the different values of width and thickness of the vibrating beam. The experiment setup is constructed as Figure-4. The width values of the vibrating beam will be used are 8mm, 10mm, 12mm and 14mm. While the thickness of the vibrating beam for each width are 1mm and 2mm. Then 80mm length of the vibrating beam is applied for all the vibrating beam. 7g of stainless-steel ball is alighted from the height of 100mm from the free end vibrating beam. The relevant between the angular acceleration and the width and thickness of the vibrating beam is illustrated in Figure-11. It indicates that for both values of thickness of the vibrating beam, the angular acceleration will be decreased as the width of the vibrating beam is broader. When the width of the vibrating beam is altered, the mass of the vibrating beam will be altered at the same time. So, the angular acceleration will be altered according to Equation (6.1).

$$\alpha = \frac{F}{mr} \tag{6.1}$$

Where F is represented as force, m is referred to mass; r is the camber path's radius and α is referred to angular acceleration. The broader the widths of the vibrating beam, the heavier the mass of the vibrating beam. Hence, the angular acceleration is reduced as the mass of the vibrating beam is increased. Consequently, the angular acceleration is inversely proportional to the mass is appropriate.

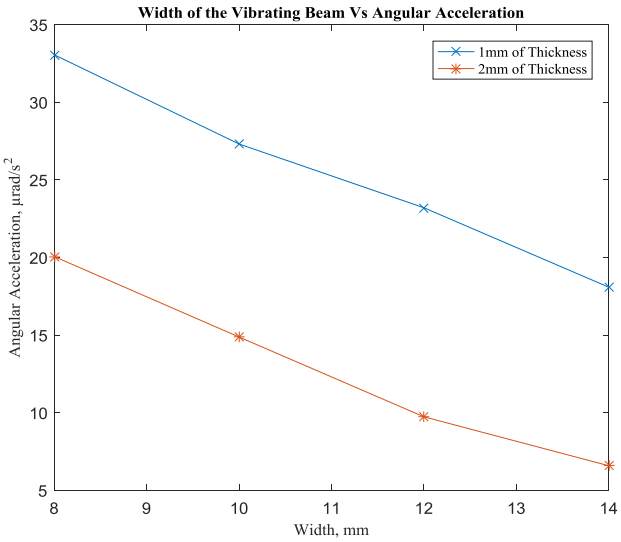

Figure-11. The angular acceleration contrast with the width by using different vibrating beam's thickness.

The stiffness against to the width of the vibrating beam is displayed in Figure-12. The stiffness of the vibrating beam is increased when the vibrating beam is broadened. According to the equation $F = kx$, the stiffness, k is inversely proportional to the linear displacement, x, and F is applied force. Based on Equations (4.1) and (6.2), the angular acceleration is directly proportional to the linear displacement due to the $\alpha \propto \theta$ and $\theta \propto S$.

$$\alpha = \frac{\theta}{t^2} \tag{6.2}$$

Thus, the linear displacement is increased when the angular displacement and the angular acceleration are increased. Thereupon, as the vibrating beam's stiffness is reduced by narrowing the vibrating beam's width, the angular acceleration is increased is denoted on Figures 11 and 12.

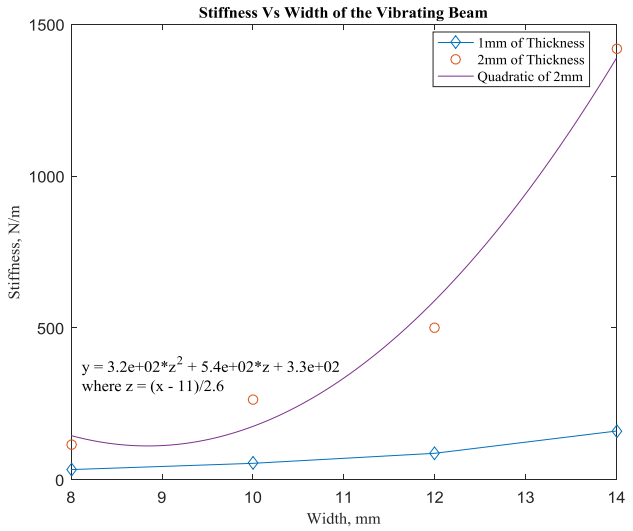

Figure-12. The stiffness against with the width by using different vibrating beam's thickness.

6.2 The Vibrating Beam is applied on the Power Generator

The tentative is carried on by enclosing the vibrating beam on the piezoelectric power generator. The tentative setup is conducted as Figures 9 and 10. The variables which are width and thickness of the vibrating beam will be utilized and altered on the power generator. The vibrating beam's width values: 8mm, 10mm, 12mm and 14mm. While the thickness values: 1mm and 2mm and 80mm of length are applied for each of the vibrating beam. A 25g weight of the proof mass and 3mm of the interfaced plate's diameter are enclosed. A 30kΩ of resistor is acted as a load resistance for the piezoelectric disc and is interfaced parallel to the piezoelectric disc. 1 G-level of the acceleration level is utilized on the electrodynamic shaker. In order to observed and record the output efficiency of the piezoelectric disc, a digital storage oscilloscope is used. 10ms of the sampling time for the output reading is set in the oscilloscope.

The differentiation of the distinct values of width and thickness for the vibrating beam to the output voltage and power response to the frequency are appraised and represented in Figures 13 and 14. The output voltage amplitude is increased as the width of the vibrating beam is narrowed is expressed in Figure 13. The maximum output voltage of 33.2V_{max} is yielded during an 8mm width and 1mm thickness of vibrating beam is applied. Next, the output voltage values are 30.5V_{max}, 29.7V_{max} and 28.9V_{max} for the 10mm, 12mm and 14mm the vibrating beam's width, respectively. This is due to the output voltage is inversely proportional to the vibrating beam's width. Based on the Equation indicated that the vibrating beam's width, w is inversely proportional to the bending stress,σ_b. Thereupon, the bending stress of the vibrating beam and the output voltage are reduced during the width of beam is broadened according to the Equation (6.3).

$$D_i = e_{ij}^{\sigma} E_j + d_{im}^{d} \sigma_m \quad (6.3)$$

Where, D_i is referred to dielectric displacement, e_{ij}^{σ} is represented as dielectric permittivity, E_j is referred to the applied electric field, d_{im}^{d} is piezoelectric coefficients and σ_m is represented as stress. As $D_i \propto \sigma_m$, the larger the stress provided to the piezoelectric disc, the higher the output voltage of the piezoelectric disc which also called as the dielectric displacement.

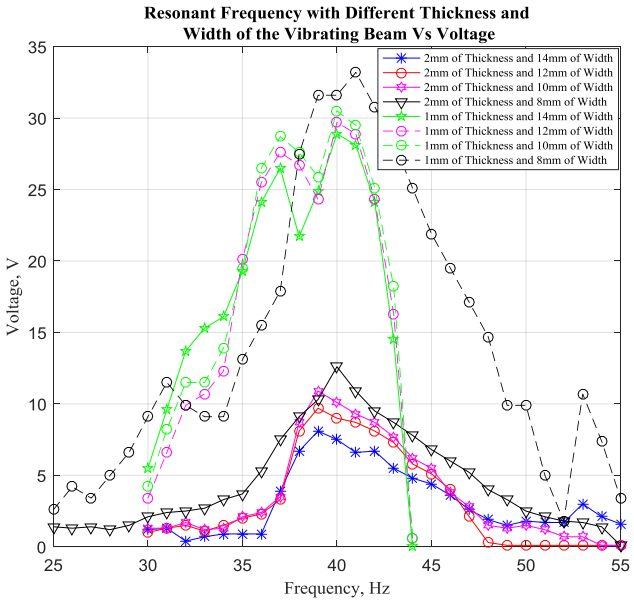

Figure-13. The output voltage contrast with the frequency with different vibrating beam's width and thickness.

The graph illustrates that output voltage is raised progressively from frequency of 25Hz to 41Hz. After that, the output amplitude is decreased gently from frequency of 41Hz to 55Hz by using the vibrating beam's width of 8mm and 1mm thickness. Whereas, for the 10mm, 12mm and 14mm width, the output voltage is raised steadily from frequency 30Hz to 40Hz. The output voltage is decreased obviously after the frequency of 40Hz. 16Hz of the operating frequency bandwidth for 8mm width is broader than the others value widths of the vibrating beam. This is believed that the 8mm width's anti-resonance is dissimilar with other width values. An anti-resonance for the system can be affected by the mass distribution, bending stress and stiffness of the system. The prerequisites that are incorporate for the bending stress of the system is explained in Equation (2.2) earlier. In addition, the vibrating beam's width can have an impact on the piezoelectric disc's frequency response as it is expressed in Equation (6.4).

$$f = \pm\sqrt{F_{impact}\left(\frac{2}{\Delta L}\right)\left(\frac{1}{4\pi^2 m_{eff}}\right)} \quad (6.4)$$

Where f is referred to frequency, the vector F_{impact} is represented as impact force, ΔL is the peak to peak of the displacement, and m_{eff} is the effective mass. The effective mass of the system is modeled as Equation (6.5).

$$m_{eff} = 0.2.36m_{syst} = 0.236\rho_{syst}w_{syst}h_{syst}l_{syst} \quad (6.5)$$

Where m_{syst} is the total mass of the system, ρ_{syst} is referred to the density of the system, w_{syst} is the width of the system, h_{syst} is represented to the thickness or height of the system and l_{syst} is the length of the system. The effective mass is directly proportional to the beam's width. Thereupon, $w \propto \frac{1}{f}$ because of the $w \propto m_{eff}$ and $m_{eff} \propto \frac{1}{f}$, where w is width of the vibrating beam. Thus, the resonant frequency of the piezoelectric disc is decreased as the vibrating beam's width is broadened.

Then, the operating frequency range for 2mm thickness of the vibrating beam is between 30Hz to 55Hz. The figure affirmed that the output efficiency of the piezoelectric disc is increased as the vibrating beam's width is decreased for 2mm thickness. The harvested output voltages are $12.6V_{max}$, $10.9V_{max}$, $9.7V_{max}$ and $8.1V_{max}$ for the 8mm, 10mm, 12mm and 14mm of vibrating beam's width, respectively. The stiffness of the beam is decreased, and the linear displacement of the beam is increased as the vibrating beam's width is reduced according to Equations (4.1) and (6.2), and plotted in Figures 11 and 12. The applied force of the screw tip on the vibrating beam contacts to the piezoelectric disc is raised when the linear displacement is raised based on the equation of $F = kx$ that is expounded before. Hence, the output voltage of the piezoelectric disc can be enhanced likewise.

Moreover, around 64% of the output voltage is reduced during the vibrating beam's thickness is changed from 1mm to 2mm is illustrated in the plotted graph. The output voltage is inversely proportional to the vibrating beam's thickness based on Equation (2.2) and (6.3) which are deliberated previously. Due to the $\sigma_b \propto \frac{1}{t}$ and $D_i \propto \sigma_m$, where σ_b and σ_m are stress, t is represented as the vibrating beam's thickness and D_i is referred to dielectric displacement.

Furthermore, the frequency response of the piezoelectric disc can be affected by the vibrating beam's thickness is clarified in the plotted graph. 40Hz and 39Hz are the resonant frequency of the piezoelectric disc when 1mm and 2mm thickness of the vibrating beam is employed, respectively. The piezoelectric disc's resonant frequency is inversely proportional to the vibrating beam's thickness. As from Equations (6.4) and (6.5) which are indicated previously, $t \propto \frac{1}{f}$ because of the $t \propto m_{eff}$ and $m_{eff} \propto \frac{1}{f}$. Where, t and h_{syst} is the thickness of the vibrating beam. Therefore, the resonant frequency of the piezoelectric disc is decreased (shifted to left side) when the vibrating beam's thickness is increased. Besides that, the operating frequency bandwidth of the piezoelectric disc for 1mm thickness of the vibrating beam is narrower than the 2mm thickness. The bandwidths of the operating frequency for 1mm and 2mm thickness of vibrating beam used are from 30Hz to 44Hz and from 30Hz to 55Hz, respectively. As the anti-resonance of the vibrating beam which is mentioned in earlier, the vibrating beam's thickness can influence the operating frequency's bandwidth. The bending stress, mass distribution and stiffness can affect on it. The variables of the bending stress can be defined in Equation (2.2).

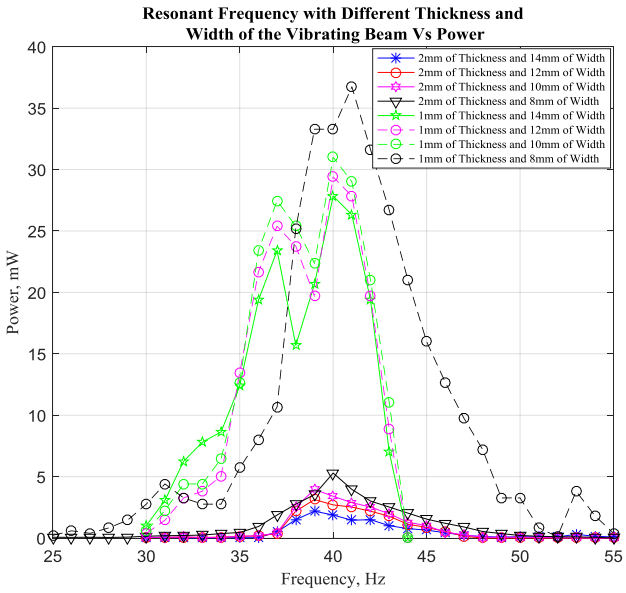

Figure-14. The output power contrast with the frequency with different vibrating beam's width and thickness.

The relationship between the output power with the frequency response of the piezoelectric disc is interpreted in Figure-14. Based on the equation of $P = VI$, so $P \propto \frac{1}{w}$ due to the $P \propto V$ and $V \propto \frac{1}{w}$. 36.74mW of maximal output power is harvested during the 8mm width and 1mm thickness of the vibrating beam is employed. Consequently, not only the output power can be influenced but the frequency responses of the piezoelectric disc can be influenced also by the vibrating beam's width. It is acknowledged in the plotted Figure-14. Moreover, 5.29mW, 3.96mW, 3.14mW and 2.19mW of output power are yielded by utilizing 8mm, 10mm, 12mm and 14mm of width and 2mm thickness of the vibrating beam, respectively. Therefore, the vibrating beam's width is inversely proportionality to the output power of the piezoelectric disc is admissible and verified by the Figures 13 and 14.

Around 87% of the output efficiency of the piezoelectric disc is declined when 1mm of vibrating beam's thickness is varied to 2mm is displayed in Figure 14, which is alike with Figure-13. In addition, the frequency responses of the piezoelectric disc are same as the Figure-13. Due to the $P = VI$, thus $P \propto V$. Therefore, the inversely proportionality of the output power and the frequency responses with the vibrating beam's thickness is adopted as the output voltage is inversely proportional to the vibrating beam's thickness. Consequently, the output power and the frequency responses of the piezoelectric disc can be influenced by the vibrating beam's thickness.

7. CONCLUSIONS

The stiffness of the vibrating beam is characterized, and the operating frequency and output efficiency of the piezoelectric disc are externalized in this paper. The stiffness of the vibrating beam is proportional to vibrating beam's width, yet, inversely proportional to the deflection of the vibrating beam. When the vibrating beam is applied on the piezoelectric power generator and 1 G-level of acceleration level is set up to the electrodynamic shaker, so that the screw tip on the vibrating beam can be contacted on the piezoelectric disc. $33.2V_{max}$ of the maximum output power is harvested when enclosing the width and thickness of the vibrating beam are 8mm and 1mm, respectively. Furthermore, the piezoelectric disc's output efficiency is inversely proportional to the stiffness of the vibrating beam. With the lowest stiffness of the vibrating beam which is 8mm width and 1mm thickness, around 87% of the output efficiency can be raised compared to the 8mm width and 2mm thickness of the vibrating beam. Moreover, the piezoelectric disc's frequency response also is inversely proportional to the stiffness of the vibrating beam. The narrower the vibrating beam's width and the thinner the vibrating beam's thickness, the higher the resonant frequency of the piezoelectric disc. In a nut shell, the vibrating beam's stiffness not merely can influence the frequency responses but the output efficiency of the piezoelectric disc as well.

ACKNOWLEDGEMENTS

The first author would like to thank UTeM Zamalah Scheme for the sponsorship scheme.

REFERENCES

[1] N. X. Yan, A. A. Basari and N. A. A. Nawir. 2018. PIEZOELECTRIC CERAMIC FOR ENERGY HARVESTING SYSTEM: A REVIEW.

[2] G. Mart inez-Ayuso, M. I. Friswell, S. Adhikari, H. H. Khodaparast and C. A. Featherston. 2017. Energy harvesting using porous piezoelectric beam with impacts. Procedia Eng. 199: 3468-3473.

[3] A. Morel, R. Grézaud, G. Pillonnet, P. Gasnier, G. Despesse and A. Badel. 2016. Active AC/DC control for wideband piezoelectric energy harvesting. in Journal of Physics: Conference Series. 773(1): 12059.

[4] Y. Bai et al. 2018. Investigation of a cantilever structured piezoelectric energy harvester used for wearable devices with random vibration input. Mech. Syst. Signal Process. 106: 303-318.

[5] M. A. Halim, S. Khym and J. Y. Park. 2013. Impact based frequency increased piezoelectric vibration energy harvester for human motion related environments. in The 8th Annual IEEE International Conference on Nano/Micro Engineered and Molecular Systems. pp. 949-952.

[6] K. V. A. K.Srikanth. 2017. State of art: Piezoelectric Vibration Energy Harvesters. Mater. Today Proc. 4(2, Part A): 1091-1098.

[7] N. M. Ali, A. A. Mustapha and K. S. Leong. 2013. Investigation of hybrid energy harvesting circuits using piezoelectric and electromagnetic mechanisms. in 2013 IEEE Student Conference on Research and Development. pp. 564-568.

[8] S. L. Kok, M. F. A. Rahman, D. F. W. Yap and Y. H. Ho. 2011. Bandwidth widening strategies for piezoelectric based energy harvesting from ambient vibration sources. in 2011 IEEE International Conference on Computer Applications and Industrial Electronics (ICCAIE). pp. 492-496.

[9] B. Y. Jing and K. S. Leong. 2018. Linearity Improvement for Cantilever Based Piezoelectric by Using Resonant Shifting Method. J. Telecommun. Electron. Comput. Eng. 10(2-7): 7-10.

[10] B. Y. Jing and K. S. Leong. 2016. Parametric Studies on Resonance Frequency Variation for Piezoelectric Energy Harvesting With Varying Proof Mass and Cantilever Length. in Journal of Telecommunication, Electronic and Computer Engineering (JTEC). 8(5): 119-123.

[11] J. Palosaari, M. Leinonen, J. Juuti, and H. Jantunen. 2018. The effects of substrate layer thickness on piezoelectric vibration energy harvesting with a bimorph type cantilever. Mech. Syst. Signal Process. 106: 114-118.

[12] T. Kumar, R. Kumar, and V. S. Chauhan. 2015. Design and finite element analysis of varying width piezoelectric cantilever beam to harvest energy. in Energy, Power and Environment: Towards Sustainable Growth (ICEPE), 2015 International Conference on. pp. 1-6.

[13] Z. Yang, Y. Q. Wang, L. Zuo and J. Zu. 2017. Introducing arc-shaped piezoelectric elements into energy harvesters. Energy Convers. Manag. 148: 260-266.

[14] A. A. Basari et al. 2014. Shape effect of piezoelectric energy harvester on vibration power generation. J. Power Energy Eng. 2014(2): 117-124.

[15] X. D. Xie, A. Carpinteri and Q. Wang. 2017. A theoretical model for a piezoelectric energy harvester with a tapered shape. Eng. Struct. 144(Supplement C): 19-25.

[16] S. Roundy et al. 2005. Improving power output for vibration-based energy scavengers. IEEE Pervasive Comput. 4(1): 28-36.

[17] N. X. Yan, A. A. Basari, K. S. Leong, N. A. A. Nawir and S. Hashimoto. 2018. Investigation and experimental verification of the effectiveness of the interfaced plate parameters on impact-based piezoelectric energy harvester. Ceram. Int. 44(15): 17724-17734.

[18] A. A. Basari, S. Hashimoto, B. Homma, H. Okada, H. Okuno and S. Kumagai. 2016. Design and optimization of a wideband impact mode piezoelectric power generator. Ceram. Int. 42(6): 6962-6968.

[19] S. Hashimoto *et al*. 20166. Evaluation of impact mode-based piezoelectric power generator. in 2016 IEEE 11th Conference on Industrial Electronics and Applications (ICIEA). pp. 1131-1134.

[20] F. P. J. S. D. L. Ashby Michael F. 2009. 4.3.1.2 Stress. Nanomaterials, Nanotechnologies and Design - An Introduction for Engineers and Architects. Elsevier.